scientific reports

Check for updates

OPEN

Mutual synchronization of spin-torque oscillators within a ring array

M. A. Castro[1], D. Mancilla-Almonacid[1], B. Dieny[2], S. Allende[1]✉, L. D. Buda-Prejbeanu[2] & U. Ebels[2]

An array of spin torque nano-oscillators (STNOs), coupled by dipolar interaction and arranged on a ring, has been studied numerically and analytically. The phase patterns and locking ranges are extracted as a function of the number *N*, their separation, and the current density mismatch between selected subgroups of STNOs. If $N \geq 6$ for identical current densities through all STNOs, two degenerated modes are identified an in-phase mode (all STNOs have the same phase) and a splay mode (the phase makes a 2π turn along the ring). When inducing a current density mismatch between two subgroups, additional phase shifts occur. The locking range (maximum current density mismatch) of the in-phase mode is larger than the one for the splay mode and depends on the number *N* of STNOs on the ring as well as on the separation. These results can be used for the development of magnetic devices that are based on STNO arrays.

Spin torque nano-oscillators (STNOs) are nanoscale signal sources that can convert a DC input signal (current or voltage) into a microwave output voltage signal[1,2]. Depending on the magnetization configuration of the polarizing and the free layer, an STNO can generate rf signals in the 100 MHz to several tens of GHz range for both configuration nanopillars and nanocontact[3–6]. An important property of STNOs is their strong coupling between the oscillation amplitude and phase[7] which enables the tuning of their frequency via the DC input signal[8,9]. Furthermore, it enables, via an additional time-varying input signal, injection locking of the STNO frequency and phase[10], modulation of the STNO amplitude, frequency or phase[11,12], or sweep-tuning of the STNO frequency[13]. These properties open a large range of potential applications such as wireless communication[12,14], ultra-fast spectrum analysis[13] as well as oscillator based hardware implementations for neuromorphic computation[15,16]. For these applications, but also from a fundamental point of view, the collective excitation states of a small or larger sized array of coupled STNOs is of interest[17,18]. Here, STNOs offer a rich variety of coupling mechanisms (e.g. electrical[19–21], dipolar[17,18,22–24] or spin pumping[25]) and coupling scenarios (long range with all-to-all coupling or short range with nearest neighbors coupling).

A general question for such coupled STNO arrays is under what conditions a stationary fully coherent dynamic state exists, for which the phases of all STNOs are correlated and for which the corresponding phase differences are constant in time (as compared to the free running state where the phases are free and uncorrelated). Other solutions for the collective state might exist such as chaotic states[19] or chimera states[21], that will depend on the number of STNOs (large arrays), the coupling type, external control parameters (current, field) as well as on the homogeneity of the STNO properties (identical STNOs vs. a dispersion of STNO parameters). These states have been observed in other systems like 2D periodic lattice of Kuramoto oscillators[26] or ring structure of identical Kuramoto oscillators[27]. Previous simulation studies on two STNOs[24], coupled through dipolar interaction, have shown that depending on the initial condition or STNO configuration, it is possible to stabilize an in-phase or anti-phase synchronised state[28–31]. Such modes can be associated with different applications, for instance, the in-phase mode is required to enhance the emission power, and the anti-phase mode can be useful for applications in phased array radar systems or bio-inspired computing[25,32]. Then, a general question is whether the number of possible phase states increases upon increasing the number N of STNOs and how to control the phase patterns via frequency mismatches. Here we make a first step in this direction, and report on the different phase states that can be obtained for a small STNO array (number $N = 4–12$) where the STNOs are arranged in a ring array, see Fig. 1. Such a ring can be viewed as a 1D line with periodic boundary conditions. We consider as the interaction type all-to-all dipolar interaction of identical STNOs and determine the solutions for the phase

[1]Universidad de Santiago de Chile (USACH), Departamento de Física, CEDENNA, Avda. V. Jara 3493, Estación Central, Santiago, Chile. [2]Univ. Grenoble Alpes, CEA, CNRS, Grenoble INP, SPINTEC, 38000 Grenoble, France. ✉email: sebastian.allende@usach.cl

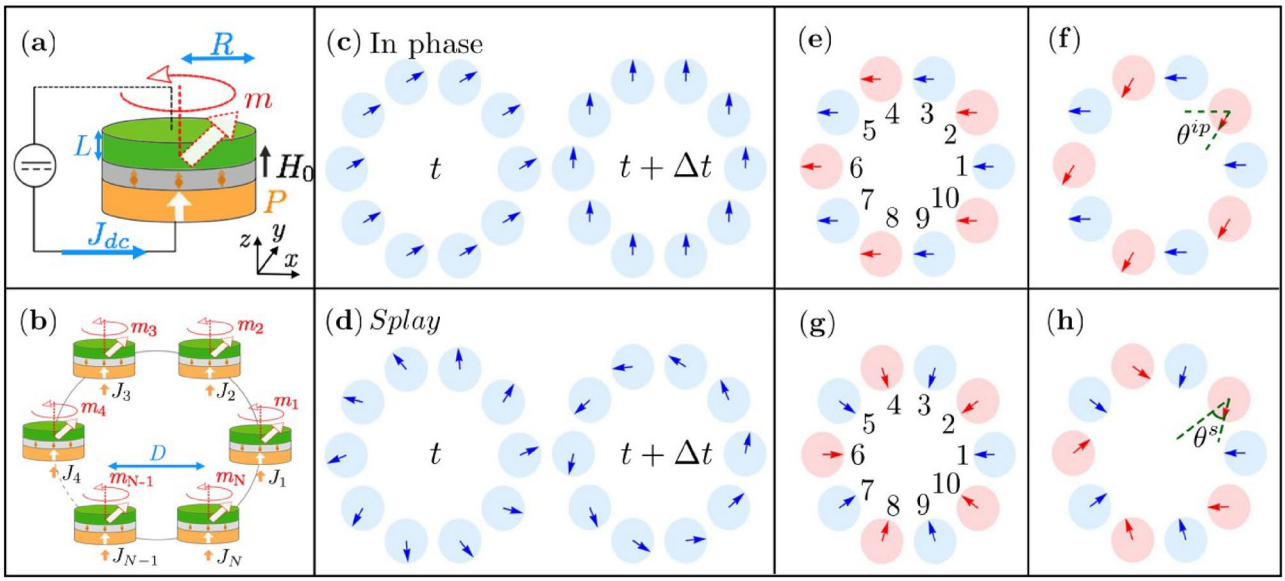

Figure 1. Schematic of (**a**) a single STNO and (**b**) an array of N STNOs distributed along a ring. Phase states of the $N = 10$ synchronized STNOs ring array for identical current densities through the STNOs: (**c**) in-phase mode and (**d**) splay mode. Phase patterns for non-identical current densities through the STNOs applied to: (**e**,**f**) the in-phase mode and (**g**,**h**) the splay mode. (**e**,**g**) are for zero current density mismatch and show the labeling of STNOs. (**f**,**h**) are for non-zero mismatch where the additional phase rotation is indicated by the angles θ^{ip} and θ^{s}. The blue color illustrates the odd (1, 3, 5...) and the red color the even (2, 4, 6...) STNO position within the ring array. In the Supplementary Material, we include four videos of the modes for the different cases: two videos for identical current densities for both modes (cases (**e**,**g**)), and two videos for non-identical current densities for both modes (cases (**f**,**h**)).

states numerically as well as analytically. When the currents are identical, we observe that in addition to the in-phase mode (all the phases equal), an additional mode appears where the phases of the oscillators are spaced equally around the ring. This state corresponds to a splay mode[33,34] which is characterized by a winding number related to the number of rotations around the ring. The splay mode that we observe corresponds to a winding number 1. Further phase states are obtained when the current density in a subgroup of STNOs is varied while it is kept constant in another subgroup.

Model

For the modeling, STNO nanopillars of circular shape with radius R and of free layer thickness L, (see Fig. 1a) are considered that support an out-of-plane precession (OPP) mode. This is achieved by a perpendicular polarizer and a free layer that is in-plane magnetized. In this case, the magnetization $\boldsymbol{M}$ oscillates around the out-of-plane z-axis[35] providing very symmetric oscillation trajectories that can be modeled analytically. Furthermore a strong out-of plane field $\boldsymbol{H}_0$ is applied to saturate the magnetization $\boldsymbol{M}$ out-of-plane in absence of current. In this way, the oscillation amplitude and with this the frequency and the dynamic dipolar interaction fields increase with increasing DC current density[36]. For the ring structure, an even number N of STNOs ($N = 4, 6, 8, 10, 12$) is considered, with a center to center distance D between two adjacent oscillators, see Fig. 1b. Upon increasing the number N, the ring diameter is increased to keep D constant. To describe the magnetization dynamics of each STNO, we use the macrospin approximation. This approximation adequately describes the magnetization dynamics for the parameters considered in this study.

The solutions for the phases of each STNO in the synchronized state were obtained by numerical simulation and are compared to analytical phase solutions. For the numerical simulations, the coupled Landau–Lifshitz–Gilbert–Slonczewski (LLGS) equations are solved, where the dynamics of the k-th free layer is described by

$$\frac{d\boldsymbol{m}_k}{dt} = -\gamma_0(\boldsymbol{m}_k \times \boldsymbol{H}^k_{eff}) + \alpha(\boldsymbol{m}_k \times \frac{d\boldsymbol{m}_k}{dt}) - \gamma_0 a_j J_k \boldsymbol{m}_k \times (\boldsymbol{m}_k \times \boldsymbol{P}),$$

where $\boldsymbol{m}_k = \boldsymbol{M}_k/M_s$ is the normalized magnetization of the k-th free layer and M_s is the saturation magnetization; $\gamma_0 = \gamma\mu_0$, γ is gyromagnetic ratio and μ_0 is the vacuum permeability; α is the damping constant; J_k is the current density on the k-th STNO; $a_j = \hbar\eta/(2e\mu_0 M_s L)$ is the spin-transfer torque parameter; $\boldsymbol{P} = \hat{\boldsymbol{z}}$ is the spin polarization direction and η the spin polarization of the current. The effective field on the k-th free layer is

$$\boldsymbol{H}^k_{eff} = H_0\hat{\boldsymbol{z}} + \boldsymbol{H}_d + \boldsymbol{H}^k_{int}, \tag{1}$$

where H_0 is the external out-of-plane field and $\boldsymbol{H}_d$ is the self-demagnetizing field, with $|\boldsymbol{H}_d| = M_s(N_z - N_x)$. N_z and N_x are the corresponding demagnetization factors of the circular free layer. $\boldsymbol{H}_{int}^k$ is the magnetostatic interaction field acting on the *k-th* free layer of the STNO due to the other free-layers. It is given by[24]

$$\boldsymbol{H}_{int}^k = M_s \sum_{l=1,l\neq k}^{N} \Big\{ \Big([K_1^{k,l} + K_2^{k,l}\cos(2\varphi_{k,l})]m_x^l + K_2^{k,l}\sin(2\varphi_{k,l})m_y^l \Big)\hat{\mathbf{x}} + \Big([K_1^{k,l} - K_2^{k,l}\cos(2\varphi_{k,l})]m_y^l + K_2^{k,l}\sin(2\varphi_{k,l})m_x^l \Big)\hat{\mathbf{y}} + K_3^{k,l} m_z^l \hat{\mathbf{z}} \Big\}, \tag{2}$$

where $\varphi_{k,l}$ is the angle between the STNOs k and l, and $K_i^{k,l} = K_i(D_{k,l})$ are functions that depend on the radius of the STNOs and on the inverse of the separation between them, see Eqs. B14 in Ref.[24] for expressions of $K_i^{k,l}$. The solutions are found for the following device and material parameters: $R = 50$ nm, $L = 3$ nm, $D = 160$ nm, $M_s = 10^6$ A/m, $\alpha = 0.02, a_j = 3.78 \times 10^{-8}$ m, and $\mu_0 H_0 = 1.2$ T. This strong field could be generate via exchange coupling of the free layer to a perpendicular bias layer[13]. The corresponding critical current density at which steady state oscillations for a single isolated STNO set in is $J_c = -0.427 \times 10^{11}$ A/m^2. In the following only values of current densities are considered for which the STNOs are in the steady state.

Results and discussion

The first case of interest is that of identical current density applied to all STNOs. We analyze the phase difference between two adjacent STNOs defined as $\Delta\phi = \phi_k - \phi_{k+1}$, where $\phi_k = \arctan(m_y^k/m_x^k)$ is the angle of the magnetization of the k-th STNO that makes with the x-axis in the XY plane. Two different phase patterns were identified by numerical LLGS integration as shown in Fig. 1c,d: (c) an in-phase mode with zero phase difference between adjacent STNOs $\Delta\phi^{ip} = \phi_k - \phi_{k+1} = 0$ and (d) a splay mode characterized by a phase difference of $\Delta\phi^s = \phi_k - \phi_{k+1} = 2\pi/N$. These two modes were obtained using as an initial condition a random distribution of the initial phases ϕ_k for each STNO. The in-phase mode is the only solution identified if the STNO number is $N < 6$. For larger arrays with $N \geq 6$, both the in-phase and splay modes are found, the in-phase mode being the most probable among them. Due to its symmetry, the splay mode is characterized by an overall zero dynamic in-plane magnetization, see Fig. 1d. Furthermore, despite the different phase patterns, the frequency and the total energy of the two modes are found to be equal within 1% accuracy.

In order to induce further phase patterns, the current densities were modified as follows (for both modes): two sub-groups of STNOs are formed, one with an odd label of STNOs $(1, 3, 5, \ldots, N-1)$ within the ring for which J_{odd} was kept constant, and one for even labels $(2, 4, 6, \ldots, N)$ of STNOs for which the current density J_{even} has been varied (blue and red circles in Fig. 1e–h, respectively), increasing and decreasing its value with respect to the odd one J_{odd}, starting from the in-phase and splay mode pattern. Inducing a current density mismatch $\Delta J = J_{even} - J_{odd}$ is equivalent to inducing a frequency mismatch $\Delta f = f_{even} - f_{odd}$ between even and odd STNOs in the free running (uncoupled) state. As shown in Fig. 2a,b, it is observed that in the synchronized state (1) the frequency and the power are the same for all STNOs and for both modes; (2) there exists an upper limit for the current density (frequency) mismatch $\Delta J(\Delta f)$ that can be identified as the locking range for full synchronization, for which the two subgroups are synchronized together and have the same frequency, see Fig. 2a,b. For mismatches larger than the locking range, the even and odd subgroups are synchronized within each other (i.e., STNOs $1, 3, \ldots, N-1$ are synchronized and STNOs $2, 4, \ldots, N$ are synchronized), but the two subgroups are no more synchronized to each other and oscillate at different frequencies and have different power, see Fig. 2a,b. This is an interesting result, meaning that it is possible to generate two independent subgroups of synchronized STNOs oscillating each one at their own frequency by imposing a specific pattern of current density distribution. Moreover, the synchronized STNOs of each subgroup are not nearest neighbors. Thus the subgroup is not a geometrical cluster, where the synchronized STNOs are located all in the same region of space, but their positions are rather intermixed. We expect that it is possible to extend this finding to more than two subgroups and to different spatial patterns of the current density mismatch.

While inside the locking range the frequency and power are the same for both modes, the phase patterns are different and evolve with increasing mismatch. As shown on Fig. 1f,h the phase differences for the in-phase (splay) mode acquire an additional phase shift θ^{ip} (θ^s) between odd (constant J_{odd}) and even (varying J_{even}) STNOs. In order to better quantify these additional phase shifts, analytical expressions were derived for the STNO phases for the two modes. These analytical expressions were obtained using the spin wave formalism[7], that transforms the normalized magnetization vector of the free layer to a complex variable $c_k = (m_x^k + im_y^k)/\sqrt{2(1+m_z^k)}$ and $c_k^\dagger = (m_x^k - im_y^k)/\sqrt{2(1+m_z^k)}$. This change of variable is usually defined through the Holstein-Primakoff transformation[7,24,37]. It is convenient to write the complex-amplitude c_k in terms of the power, p_k, and phase ϕ_k of oscillation, using $c_k = \sqrt{p_k}e^{i\phi_k}$. By applying these definitions to the Eq. (1) and neglecting the non-resonant terms, it is possible to write $2N$ coupled equations for the power and phase of oscillation

$$\dot{p}_k + 2\Gamma_{eff}^k(p_k)p_k = -\sum_{l=1,k\neq l}^{N} \Omega_{k,l}\sqrt{p_k p_l}[2 - (p_k + p_l)]\sin(\phi_k - \phi_l), \tag{3}$$

$$\dot{\phi}_k + \omega_k(p_k) = -\sum_{l=1,k\neq l}^{N} \frac{\Omega_{k,l}}{2}\sqrt{\frac{p_l}{p_k}}\left[2 - (3p_k + p_l)\right]\cos(\phi_k - \phi_l). \tag{4}$$

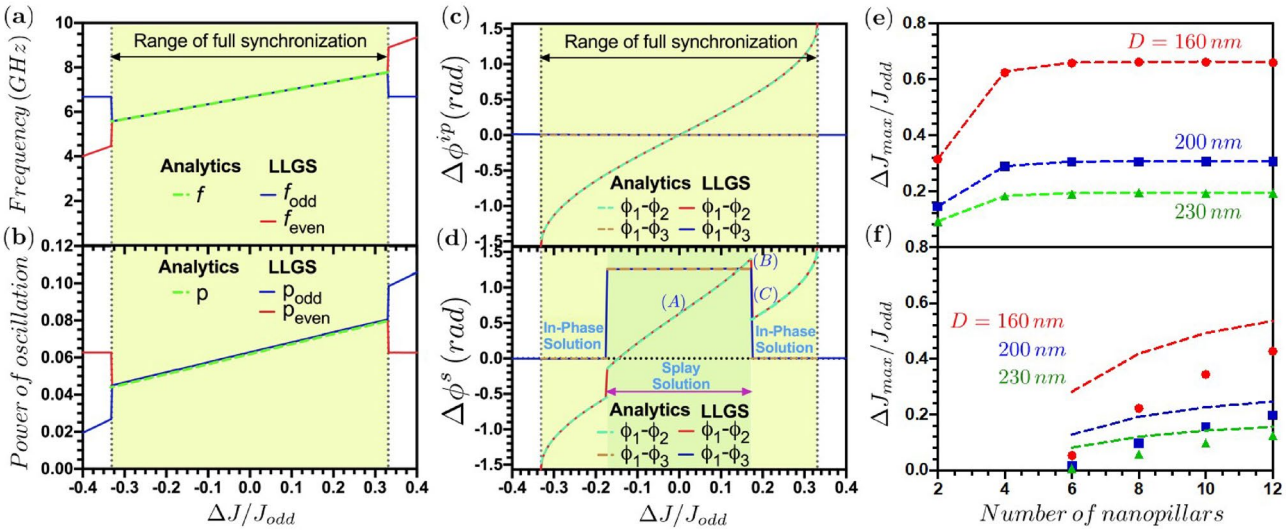

Figure 2. Dependence of (**a**) the frequency and (**b**) the power of oscillation on the normalized current density mismatch $\Delta J/J_{odd}$ with $J_{odd} = -1 \times 10^{11}\,\mathrm{A/m^2}$. In the macrospin simulations first the in-phase or splay modes were established at zero mismatch and then J_{even} was varied. Both modes result in the same frequency and power vs. mismatch (up to 1% accuracy). Phase difference $\Delta\phi$ as a function of the current density mismatch, when starting the system (**c**) in the in-phase and (**d**) the splay state. For the subfigures (**a**–**d**), we consider $N = 10$ and $D = 160$ nm; and the vertical gray dotted-lines indicate the limits of the full synchronisation range, where the phase difference between the closest STNOs is $\pm\pi/2$, see Eq. (13). The point (A) in (**d**) represents the starting-point of the macrospin simulations when the current density mismatch is zero. The point (B) in (**d**) corresponds to the transition between the splay to the in-phase solutions ($J_{even} = -1.174 \times 10^{11}\,\mathrm{A/m^2}$). The point (C) in (**d**) corresponds to the situation when the phase difference between the STNOs follows the in-phase solution. Locking range in terms of maximum current density mismatch for (**e**) the in-phase mode and (**f**) the splay mode as a function of the number N of STNOs and for different separations D between STNOs. Full dots are results from the numerical simulations and the dashed lines join the analytical solutions and guide the eye.

Here $\Gamma^k_{eff}(p_k) = \Gamma^k_+(p_k) - \Gamma^k_-(p_k)$ is the non-linear effective damping, $\Gamma^k_+(p_k)$ and $\Gamma^k_-(p_k)$ are terms related to the dissipation of energy and the injection of energy induced by the spin current, respectively; $\omega_k(p_k)$ is the nonlinear frequency and $\Omega_{k,l}$ is the coupling constant that depends on the center-to-center distance $D_{k,l}$ between the STNOs k and l. It is defined as:

$$\Omega_{k,l} = \frac{M_s\gamma_0}{\sqrt{1+\alpha^2}} K_1(D_{k,l}) \approx M_s\gamma_0 K_1(D_{k,l}). \tag{5}$$

The non-linear parameters of Eqs. (3) and (4) are defined as follows:

$$\begin{aligned} \omega^k(p) &= \omega_0^k + p^k\mathcal{N} \\ \omega_0^k &= \frac{\gamma_0}{1+\alpha^2}(H_d - H_0 - M_s \sum_{l=1,l\neq k}^{N} K_3^{k,l}) \\ \mathcal{N} &= -\frac{2\gamma_0}{1+\alpha^2} H_d \end{aligned} \tag{6}$$

$$\begin{aligned} \Gamma^k_+(p_k) &= -\frac{\gamma_0\alpha}{1+\alpha^2}\left(H_d - H_0 - M_s \sum_{l=1,l\neq k}^{N} K_3^{k,l}\right) + \frac{\gamma_0\alpha}{1+\alpha^2}((-H_0+3H_d)p_k - 2H_d p_k^2) \\ \Gamma^k_-(p_k) &= -\frac{\gamma_0 a_j J_k}{1+\alpha^2}(1-p_k). \end{aligned} \tag{7}$$

In general, it is difficult to find an analytic solution to the system of Eqs. (3) and (4) since they are strongly coupled. However, when the system is fully synchronized, the power of oscillations is practically constant and the same for each STNO as confirmed from the numerical simulations (see Fig. 2b, full lines).

Then, setting $p_k = p$ and $dp/dt = 0$, it is possible to re-write the system of Eqs. (3) and (4) as follows

$$\Gamma^k_{eff}(p) = -(1-p) \sum_{l=1,k\neq l}^{N} \Omega_{k,l} \sin(\phi_k - \phi_l), \tag{8}$$

$$\frac{d\phi_k}{dt} + \omega_k(p) = -(1-2p)\sum_{l=1,k\neq l}^{N} \Omega_{k,l}\cos(\phi_k - \phi_l). \tag{9}$$

When the STNOs are fully-synchronized, we obtain the condition $\sum_{k=1}^{N} \Gamma_{eff}^{k}(p) = 0$ from the Eq. (8), and then, the power of oscillations is given by

$$p = -[a_j J_{av} + \alpha(H_0 - H_d)]/(2\alpha H_d), \tag{10}$$

where $J_{av} = (J_{odd} + J_{even})/2$. This is the same relation as for the power of a single oscillator, replacing the current density J by the average J_{av}.

When the current density J_{even} varies, the in-phase (ip) mode and splay (s) mode satisfy respectively:

$$\phi_k^{ip} - \phi_{k+2}^{ip} = 0, \quad \phi_k^{ip} - \phi_{k+1}^{ip} = (-1)^k\theta^{ip}, \tag{11}$$

$$\phi_k^{s} - \phi_{k+2}^{s} = \frac{4\pi}{N}, \quad \phi_k^{s} - \phi_{k+1}^{s} = \frac{2\pi}{N} + (-1)^k\theta^{s}. \tag{12}$$

By using Eqs. (11) and (12) in Eq. (8), we obtain an expression for the additional phase shifts

$$\theta^{ip/s} = \arcsin\left(\frac{\gamma_0 a_j \Delta J}{2\sum_{k=1}^{N/2}\Omega_{1,2k} g^{ip/s}(k)}\right), \tag{13}$$

where $g^{ip}(k) = 1$ and $g^{s}(k) = \cos[2\pi(2k-1)/N]$. These solutions are Adler-type equations[38] and exist if the argument of the arcsin function in Eq. (13) is smaller than 1 in absolute value.

Equation (9), also provides an expression for the frequencies of the STNOs for the in-phase (f^{ip}) and splay (f^{s}) synchronization modes, where $2\pi f = d\phi/dt$

$$f^{ip/s} = -a_j\gamma_0\frac{J_{av}}{2\pi\alpha} - \gamma_0\frac{(a_j J_{av} + \alpha H_0)}{2\pi\alpha}\sum_{k=2}^{N}\frac{\Omega_{1,k}}{\gamma_0 H_d}\cos(\phi_1^{ip/s} - \phi_k^{ip/s}) \ .$$

The frequencies f^{ip} and f^{s} are practically identical. The second term of the right side is related to the interaction and it is proportional to $\Omega_{1,k}/(\gamma_0 H_d) \sim 10^{-4}$ for next nearest neighbors ($k = 2$) and for the parameters used here. This term can be neglected. As a consequence the in-phase and splay modes have the same frequency f(Eq. 14), that is, similar to the power (Eq. 10), the same expression as for a single oscillator replacing the current density by the average of the two current densities. With this the frequency is also independent of the relative phases of the dynamic magnetization between adjacent STNOs.

$$f \approx -a_j\gamma_0 J_{av}/(2\pi\alpha). \tag{14}$$

This analytical derivation is in good agreement with numerical simulation results, see Fig. 2a,b, where the frequency and power of oscillations are shown to vary linearly with the current density mismatch.

In the following, the analytical expressions for the phases Eq. (13) are analyzed in more detail and are compared to the results of the numerical simulations for the example of $N = 10$ and a constant current density $J_{odd} = -1 \times 10^{11}\mathrm{A/m^2}$ for odd STNOs. Figure 2c,d shows the phase differences between the odd and even oscillator subgroups as a function of the normalized current density mismatch obtained from the LLGS numerical solution (full lines) and the analytical solutions (dashed lines). Figure 2c,d show the phase differences when the system evolves respectively from the zero-mismatch (ΔJ =0) in-phase or splay mode. As can be seen from Fig. 2c in the case of the in-phase mode, the phase difference between all odd STNOs (1,3,5) is zero, while between the even and odd subgroups it is zero only for zero mismatch. For non-zero mismatch the phase differences follow an arcsine behaviour, Eq. (13) within the locking range (the green region in Fig. 2c). At the locking boundary where the synchronization between the two subgroups is lost, the phase difference is $\pm\pi/2$. Beyond this range, the system is partially synchronized. The results for the phase difference from the analytical and the numerical simulations are in good agreement, and therefore, we demonstrated the validity of the analytical expression.

When the system starts in the splay state, see point A in Fig. 2d, we can distinguish two locking ranges. First, for zero mismatch, the phase difference between neighboring even and odd STNOs is non-zero and takes the value of $2\pi/N = 0.63$rad (Eq. 12). Increasing the mismatch, the phase of the even STNOs acquires an additional phase shift as given by Eq. (13) with an arcsine dependence as a function of mismatch. In this range the results from numerical simulations and the analytical expressions agree well. The simulations show, that at a certain critical value of the current density mismatch (see point B in Fig. 2d, the splay mode becomes unstable and transits irreversibly into the in-phase mode characterized by the phase differences defined by Eq. (11) (see point C in Fig. 2d, until the phase difference between the even and odd STNO subgroups reaches $\pm\pi/2$ and the two subgroups are no more synchronized. Decreasing then the current density mismatch, the system remains in the in-phase mode and it is not possible to return to the splay state. It is noted, that the analytical solutions lead to a somewhat larger value for the critical current density mismatch where the splay mode transits to the in-phase mode.

From the analytical expressions Eq. (13), one can derive an expression for the locking range of the in-phase mode. Synchronization is lost when the phase difference between the even and odd subgroups becomes $\theta^{ip} = \pi/2$. This leads to:

$$(J_{max} - J_{min}) = \frac{4}{a_j \gamma_0} \sum_{k=1}^{N/2} \Omega_{1,2k}. \tag{15}$$

Similar to injection locking of an oscillator to an external signal, the locking range here depends strongly on the coupling constant $\Omega_{k,l}$. It increases with the coupling, and thus Eq. (15) is the equivalent to Arnold tongue boundaries. Furthermore, Eq. (15) shows that the locking depends on the sum over dipolar interactions, and it is thus expected to increase with increasing number N of STNOs in the ring. This is confirmed in Fig. 2e, where the locking range is shown vs. N from numerical and analytical calculations. Both agree well and show first an increase up to $N = 4$ and then a saturation. This seems to suggest that only next nearest neighbor interaction are important. However, from additional simulations (not shown here) we have seen that for instance that for next nearest neighbor interaction a mode with winding number 2 can exist which is unstable when all to all interactions are considered. Hence, to correctly describe the dynamics of the ring configuration, a larger range of STNO interaction needs to be considered. Finally, since the dipolar interaction increases with decreasing separation D between STNOs, the locking range strongly increases upon reducing D, as can be seen in Fig. 2e. These results also are valid for large separation between the STNOs, since the dipolar coupling decreases. On the other hand, for small separation i.e., edge to edge separation equal to 50 nm, we have checked that our equations are still valid. It is noted though that experimentally edge-edge distances below 50 nm are hard to achieve. From the numerical simulations, we have also extracted the current density mismatch where the splay mode transits to the in-phase mode. The corresponding locking ranges show a strong increase with the number N of STNOs, see Fig. 2f, and a strong increase for decreasing separation. We observe that the analytical threshold for the splay mode is an overestimation as the numerical simulations show a switch to the in-phase mode before the theoretical threshold. The difference between the analytical and numerical results is explained through the fact that the theoretical expression of Eq. (13) provides only the existence condition for the solution but it does not provide any conditions for the stability of the solution. This would require further analysis doing a stability analysis similar to Ref.[27]. Finally, we want to remark that our calculations were done at zero temperature because our main goal was to understand the synchronization of this system when there is magnetostatic interaction among the STNOs. A possible future study would be to include temperature and determine how thermal fluctuations affect the synchronization of these systems.

Conclusions

To conclude, we have studied theoretically the phase patterns that can be obtained for an array of STNOs arranged on a ring array and coupled via dipolar interaction. When the same current density is applied to all STNOs, two different synchronized modes are observed, the in-phase mode for which all STNOs have the same phase, and the splay mode where the phase makes a 2π turn along the ring array. The latter is observed only when the number N of STNOs within the ring is larger or equal to $N = 6$. Further phase patterns were obtained when varying the current density in a subgroup of STNOs, where all even STNOs formed the subgroup. For the in-phase mode, a current density mismatch (equivalent to a frequency mismatch), the two even and odd STNO subgroups remain synchronized within a certain synchronization range whose size scales with the dipolar interactions. Beyond this locking range, the two sub-groups de-synchronize, but the STNOs remain synchronized within each subgroup. The existence range of the splay mode is smaller than the in-phase synchronization range. Thus, a critical current density mismatch exists, where the splay mode becomes unstable and transits to the in-phase mode. Finally, despite the different phase patterns of the in-phase and splay mode (that lead to different dynamic dipolar interactions between adjacent STNOs), the frequency and power of the STNOs are the same inside the full synchronization range. The numerical results are confirmed from analytical results obtained by solving the phase equations of the coupled STNO array. Expressions have been provided for the ring array for the phase equation, the phase shifts as a function of current density mismatch, the power, frequency and Arnold tongue boundaries. We show that the amplitude and the frequency at which the system synchronizes depend on the average current density supplied to the system and the applied magnetic field. This is an interesting feature indicating that the effect of magnetostatic interaction on the amplitude and frequency of oscillations can be neglected in such symmetric coupled system. It is expected that upon increasing the number N of STNOs within the array for identical current densities, it should be possible to induce further phase patterns, where the phase makes more than one turn along the ring. Furthermore, it is expected that a large variety of different phase patterns can be induced by choosing different subgroups of STNOs, for which the current density is varied. For different concepts for neuro-inspired computing based on coupled oscillators, one needs to understand how the collective state of interacting STNOs changes as a function of external control parameters. For STNOs such a control parameter can be an applied DC current or DC field. The present results of this article are the first step in this direction, demonstrating that the collective state can change from the splay to the in-phase mode upon variation of the current through a subset of devices. An abrupt change of the collective state as a function of control parameter can also be used to realize sensor devices.

Received: 24 November 2021; Accepted: 12 May 2022
Published online: 14 July 2022

References

1. Slonczewski, J. Current-driven excitation of magnetic multilayers. *J. Magn. Magn. Mater.* **159**, L1–L7. https://doi.org/10.1016/0304-8853(96)00062-5 (1996).
2. Chen, T. *et al.* Spin-torque and spin-hall nano-oscillators. *Proc. IEEE* **104**, 1919–1945. https://doi.org/10.1109/JPROC.2016.2554518 (2016).
3. Puliafito, V., Consolo, G., Lopez-Diaz, L. & Azzerboni, B. Synchronization of propagating spin-wave modes in a double-contact spin-torque oscillator: A micromagnetic study. *Phys. B Condensed Matter* **435**, 44–49. https://doi.org/10.1016/j.physb.2013.09.042 (2014).
4. Houshang, A. *et al.* Spin-wave-beam driven synchronization of nanocontact spin-torque oscillators. *Nat. Nanotechnol.* **11**, 280–286. https://doi.org/10.1038/nnano.2015.280 (2016).
5. Consolo, G. *et al.* Combined frequency-amplitude nonlinear modulation: Theory and applications. *IEEE Trans. Magn.* **46**, 3629–3634. https://doi.org/10.1109/TMAG.2010.2046178 (2010).
6. Muduli, P. K., Ye. Pogoryelov, F. . M. & Akerman, J. Modulation of individual and mutually synchronized nanocontact-based spin torque oscillators. *IEEE Trans. Magn.* **47**, 1575–1579. https://doi.org/10.1109/TMAG.2010.2096463 (2011).
7. Slavin, A. & Tiberkevich, V. Nonlinear auto-oscillator theory of microwave generation by spin-polarized current. *IEEE Trans. Magn.* **45**, 1875–1918. https://doi.org/10.1109/TMAG.2008.2009935 (2009).
8. Kiselev, S. I. *et al.* Microwave oscillations of a nanomagnet driven by a spin-polarized current. *Nature* **425**, 380–383. https://doi.org/10.1038/nature01967 (2003).
9. Rippard, W. H., Pufall, M. R., Kaka, S., Russek, S. E. & Silva, T. J. Direct-current induced dynamics in $co_{90}fe_{10}/ni_{80}fe_{20}$ point contacts. *Phys. Rev. Lett.* **92**, 027201. https://doi.org/10.1103/PhysRevLett.92.027201 (2004).
10. Rippard, W. H. *et al.* Injection locking and phase control of spin transfer nano-oscillators. *Phys. Rev. Lett.* **95**, 067203. https://doi.org/10.1103/PhysRevLett.95.067203 (2005).
11. Pufall, M. R., Rippard, W. H., Kaka, S., Silva, T. J. & Russek, S. E. Frequency modulation of spin-transfer oscillators. *Appl. Phys. Lett.* **86**, 082506. https://doi.org/10.1063/1.1875762 (2005).
12. Litvinenko, A. *et al.* Analog and digital phase modulation and signal transmission with spin-torque nano-oscillators. *Phys. Rev. Appl.* **16**, 024048. https://doi.org/10.1103/PhysRevApplied.16.024048 (2021).
13. Litvinenko, A. *et al.* Ultrafast sweep-tuned spectrum analyzer with temporal resolution based on a spin-torque nano-oscillator. *Nano Lett.* **20**, 6104–6111. https://doi.org/10.1021/acs.nanolett.0c02195 (2020).
14. Choi, H. S. *et al.* Spin nano-oscillator-based wireless communication. *Sci. Rep.* **4**, 5486. https://doi.org/10.1038/srep05486 (2014).
15. Grollier, J. *et al.* Neuromorphic spintronics. *Nat. Electron.* **3**, 360–370. https://doi.org/10.1038/s41928-019-0360-9 (2020).
16. Yogendra, K., Fan, D. & Roy, K. Coupled spin torque nano oscillators for low power neural computation. *IEEE Trans. Magn.* **51**, 1–9. https://doi.org/10.1109/TMAG.2015.2443042 (2015).
17. Lebrun, R. *et al.* Mutual synchronization of spin torque nano-oscillators through a long-range and tunable electrical coupling scheme. *Nat. Commun.* **8**, 15825. https://doi.org/10.1038/ncomms15825 (2017).
18. Tsunegi, S. *et al.* Scaling up electrically synchronized spin torque oscillator networks. *Sci. Rep.* **8**, 13475. https://doi.org/10.1038/s41598-018-31769-9 (2018).
19. Tiberkevich, V., Slavin, A., Bankowski, E. & Gerhart, G. Phase-locking and frustration in an array of nonlinear spin-torque nano-oscillators. *Appl. Phys. Lett.* **95**, 262505. https://doi.org/10.1063/1.3278602 (2009).
20. Turtle, J. *et al.* Gluing bifurcations in coupled spin torque nano-oscillators. *J. Appl. Phys.* **113**, 114901. https://doi.org/10.1063/1.4795266 (2013).
21. Zaks, M. & Pikovsky, A. Chimeras and complex cluster states in arrays of spin-torque oscillators. *Sci. Rep.* **7**, 4648. https://doi.org/10.1038/s41598-017-04918-9 (2017).
22. Abreu Araujo, F. *et al.* Optimizing magnetodipolar interactions for synchronizing vortex based spin-torque nano-oscillators. *Phys. Rev. B* **92**, 045419. https://doi.org/10.1103/PhysRevB.92.045419 (2015).
23. Flovik, V., Macià, F. & Wahlström, E. Describing synchronization and topological excitations in arrays of magnetic spin torque oscillators through the kuramoto model. *Sci. Rep.* **6**, 32528. https://doi.org/10.1038/srep32528 (2016).
24. Mancilla-Almonacid, D., Arias, R. E., Escobar, R. A., Altbir, D. & Allende, S. Spin wave modes of two magnetostatic coupled spin transfer torque nano-oscillators. *J. Appl. Phys.* **124**, 162102. https://doi.org/10.1063/1.5040262 (2018).
25. Taniguchi, T. Synchronization of spin-torque oscillators via spin pumping. *AIP Adv.* **9**, 035310. https://doi.org/10.1063/1.5066560 (2019).
26. Sarkar, M. & Gupte, N. Phase synchronization in the two-dimensional kuramoto model: Vortices and duality. *Phys. Rev. E* **103**, 032204. https://doi.org/10.1103/PhysRevE.103.032204 (2021).
27. Dénes, K., Sándor, B. & Néda, Z. Pattern selection in a ring of kuramoto oscillators. *Commun. Nonlinear Sci. Numer. Simul.* **78**, 104868. https://doi.org/10.1016/j.cnsns.2019.104868 (2019).
28. Taniguchi, T., Tsunegi, S. & Kubota, H. Mutual synchronization of spin-torque oscillators consisting of perpendicularly magnetized free layers and in-plane magnetized pinned layers. *Appl. Phys. Express* **11**, 013005. https://doi.org/10.7567/apex.11.013005 (2017).
29. Wang, C.-Z., Xu, H.-Y., Rizzo, N. D., Kiehl, R. A. & Lai, Y.-C. Phase locking of a pair of ferromagnetic nano-oscillators on a topological insulator. *Phys. Rev. Appl.* **10**, 064003. https://doi.org/10.1103/PhysRevApplied.10.064003 (2018).
30. Taniguchi, T. Phase dynamics of oscillating magnetizations coupled via spin pumping. *Phys. Rev. B* **97**, 184408. https://doi.org/10.1103/PhysRevB.97.184408 (2018).
31. Nakada, K., Yakata, S. & Kimura, T. Noise-induced synchronization in spin torque nano oscillators. *J. Appl. Phys.* **111**, 07C920. https://doi.org/10.1063/1.3680537 (2012).
32. Kudo, K. & Morie, T. Self-feedback electrically coupled spin-hall oscillator array for pattern-matching operation. *Appl. Phys. Express* **10**, 043001. https://doi.org/10.7567/apex.10.043001 (2017).
33. Matheny, M. H. *et al.* Exotic states in a simple network of nanoelectromechanical oscillators. *Science* **363**, eaav7932. https://doi.org/10.1126/science.aav7932 (2019).
34. Emenheiser, J. *et al.* Patterns: Of patterns of synchronization Noise induced attractor switching in rings of coupled nonlinear oscillators. *Chaos Interdiscip. J. Nonlinear Sci.* **26**, 094816. https://doi.org/10.1063/1.4960191 (2016).
35. Houssameddine, D. *et al.* Spin-torque oscillator using a perpendicular polarizer and a planar free layer. *Nat. Mater.* **6**, 447–453. https://doi.org/10.1038/nmat1905 (2007).
36. Zhu, J.-G., Zhu, X. & Tang, Y. Microwave assisted magnetic recording. *IEEE Trans. Magn.* **44**, 125–131. https://doi.org/10.1109/TMAG.2007.911031 (2008).
37. Rezende, S. M., de Aguiar, F. M. & Azevedo, A. Magnon excitation by spin-polarized direct currents in magnetic nanostructures. *Phys. Rev. B* **73**, 094402. https://doi.org/10.1103/PhysRevB.73.094402 (2006).
38. Pikovsky, A. *et al. Synchronization: A Universal Concept in Nonlinear Sciences. Cambridge Nonlinear Science Series* (Cambridge University Press, 2001).

Acknowledgements

We acknowledge financial support in Chile from FONDECYT Grants no. 1200867 and 1190727, and Financiamiento Basal para Centros Científicos y Tecnológicos de Excelencia AFB180001. D.M.-A. acknowledges

Postdoctorado FONDECYT 3180416 2018 and Proyecto Postdoc DICYT, Código 042131AP POSTDOC, Vicerrectoría de Investigación, Desarrollo e Innovación. M.A. Castro acknowledges Conicyt-PCHA/Doctorado Nacional/2017-21171016. This work was supported in part by the ERC Grant MAGICAL (N^{o}669204).

Author contributions

D.M.-A., S.A., B.D., L.D.B.-P., and U.E. conceived the study; M.A.C. performed the numerical calculations; M.A.C. and D.M.-A. performed the analytical calculations; M.A.C., D.M.-A., S.A., L.D.B.-P, and U.E. prepared the figures; M.A.C., D.M.-A., S.A., L.D.B.-P., and U.E. discussed the results and wrote the manuscript. All the authors reviewed the manu script.

Competing interests

The authors declare no competing interests.

Additional information

Supplementary Information The online version contains supplementary material available at https://doi.org/10.1038/s41598-022-15483-1.

Correspondence and requests for materials should be addressed to S.A.

Reprints and permissions information is available at www.nature.com/reprints.

Publisher's note Springer Nature remains neutral with regard to jurisdictional claims in published maps and institutional affiliations.